Linear Unsteady Aerodynamic Models from Wind Tunnel Measurements

Steven L. Brunton*, Clarence W. Rowley†
Princeton University, Princeton, NJ 08544

David R. Williams‡
Illinois Institute of Technology, Chicago, IL, 60616

Linear unsteady aerodynamic models are obtained for a NACA 0006 airfoil in a wind tunnel experiment at Reynolds number 65,000. A family of system identification maneuvers, based on a canonical step-up, hold maneuver, are specifically designed to extract relevant unsteady information from phase averaged wind tunnel measurements. Linear models based on these maneuvers are constructed using OKID/ERA for the case of pitching about $\alpha_0 = 0^\circ$ and $\alpha_0 = 10^\circ$, as well as the case of pure plunge. It is shown that the identified models are more accurate than Theodorsen's model for all maneuvers, especially those at larger base angle of attack.

Nomenclature

α	=	Angle-of-attack of airfoil
α_0	=	Base angle to linearize about
c	=	Chord length of airfoil
U_∞	=	Free-stream velocity
ρ	=	Fluid density
L	=	Lift force
$C_L = 2L/\rho U_\infty^2 S$	=	Lift coefficient
S	=	Surface area of airfoil
C_{L_α}	=	Lift coefficient slope in α
$\mathcal{H}_i$	=	Markov parameters from impulse response
$\mathrm{Re} = cU_\infty/\nu$	=	Reynolds number
(A_r, B_r, C_r)	=	Reduced order state-space realization of order r for fast dynamics
r	=	Order of reduced order model
$\mathbf{x}$	=	State variable for fast dynamics
$G(s)$	=	Transfer function representation of fast dynamics

I. Introduction

The need for accurate, efficient aerodynamic models has been a key motivation in research efforts over the past century. Aerodynamic models are necessary tools in the design of aircraft and to evaluate aeroelastic and flight dynamic stability. Recent studies indicate that the enhanced performance in bio-locomotion[1,2] is due to utilization of unsteady aerodynamic mechanisms. These biological observations coupled with advances

*Graduate Student, Mechanical and Aerospace Engineering. Student member, AIAA.
†Associate Professor, Mechanical and Aerospace Engineering. Associate Fellow, AIAA.
‡Professor, Mechanical, Materials, & Aerospace Engineering. Associate Fellow, AIAA.

in small-scale manufacturing techniques and feedback control design have opened up new and interesting problems in unsteady aerodynamic research.

There is a wide range of unsteady aerodynamic models in the literature. However, the classical unsteady models of Wagner[3] and Theodorsen[4] provide a benchmark for the linear models that follow them. Wagner's model constructs the lift in response to arbitrary input motion by convolving the time derivative of the motion with the analytically computed step response. Theodorsen developed an equivalent model in the frequency domain using the same model assumptions of an incompressible, inviscid, planar wake. Although Theodorsen's model only applies to sinusoidal inputs, it was more suitable for the analysis of flutter instability with the tools available at the time. However, it is possible with modern tools to construct a state space realization based on Theodorsen's model that is useful for time domain analysis.[5] Even so, both models are limited by the rigid assumptions that allow for them to be solved in closed form with analytic techiniques.

Linear indicial response models are a more general class of aerodynamic models, which may be constructed based on analytical, experimental, or numerical step response information. Wagner's model is an indicial response model based on an analytical step response. A fundamental limitation of indicial response models is their formulation based on the convolution integral, which does not fit nicely into the modern framework for feedback control design. Recently, a modeling procedure has been developed to construct low-dimensional state-space models based on the indicial (step) response.[6,7] The quasi-steady and added-mass forces that dominate at low and high frequencies, respectively, are modeled using stability derivatives, and the remaining fast dynamics are modeled using the eigensystem realization algorithm (ERA).[8,9] It is possible to use the Observer/Kalman filter identification (OKID) method[10,11] to reconstruct the indicial response from input/output data obtained from simulations, experiments, or flight tests using real maneuvers.

In this work, we demonstrate the utility of the modeling procedure outlined in Brunton and Rowley[6,7] for identifying aerodynamic models using measurements from a wind tunnel experiment. We develop a family of system identification maneuvers for use with OKID/ERA that excite unsteady aerodynamics at a range of relevant frequencies.

In section II we discuss the experiment, system identification maneuvers, and modeling procedure. Section III are the results showing the maneuvers and models for pitching about $\alpha_0 = 0^\circ$ and $\alpha_0 = 10^\circ$ and for pure plunge. Results include comparison with Theodorsen's model.

II. Methods

A. Wind Tunnel Experiment

The following experimental data was collected in the Andrew Fejer Unsteady Flow Wind Tunnel at the Illinois Institute of Technology. The wind tunnel test section is .6m $\times$ .6m $\times$ 3.5m.

The model is a NACA 0006 airfoil, shown in Figure 1, with a chord length of .246 m and span of .598 m. The free stream velocity is 4.00 m/s, which results in a Reynolds number of approximately $65,000$ and a convective time unit of .0615 seconds. In all pitching experiments the pitch point is $x/c = .11$, or 11% chord.

Forces and moments are measured using the 6$-$axis ATI Nano25 force transducer, and free stream velocity is measured using a Pitot tube with a Validyne DP-103 pressure transducer. The model is actuated using two Copley servo tubes connected to individual pushrods, allowing for a full range of pitch and heave motions. The position of these pushrods is measured using linear potentiometers.

Because the force transducer moves with the body, forces are measured in the body-fixed frame of the airfoil. Therefore, we rotate the normal (N) and parallel (P) forces in the $z-$ and $x-$ directions into the lift (L) and drag (D) forces relative to the free stream velocity according to the following:

$$\begin{bmatrix} L \\ D \end{bmatrix} = \begin{bmatrix} \cos(\alpha) & -\sin(\alpha) \\ \sin(\alpha) & \cos(\alpha) \end{bmatrix} \begin{bmatrix} N \\ P \end{bmatrix} \tag{1}$$

The pushrods are connected to the airfoil and force balance via a platform with a hinge constraint. In this way, it is possible to command an angle of attack α by varying the relative displacement of the two pushrods, as seen in Figure 1. For the pitching experiments below, we hold the front pushrod fixed, and vary the height y_1 of the rear pushrod to vary α. The vertical displacement y_1 for a given α may be solved using the following relationship:

$$(l_3 \cos(\alpha) - l_1)^2 + (-l_3 \sin(\alpha) - y_1)^2 - l_2^2 = 0 \tag{2}$$

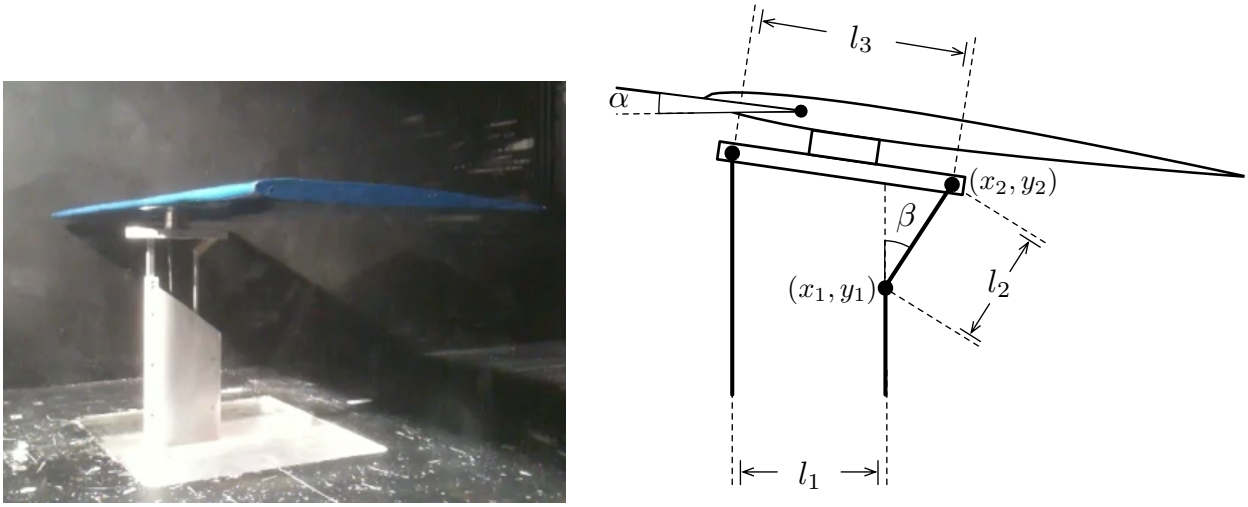

Figure 1. (left) Image of NACA 0006 model in wind tunnel. (right) Schematic of hinge apparatus connecting pushrods to platform.

where $l_1 = 2.1$", $l_2 = 1.25$", and $l_3 = 3$".

Finally, the inertia of the model, sting and pushrods introduces time lags, so the measured angle is not exactly the same as the commanded angle. Additionally, the Copley servo tube controller has its own PID dynamics. Figure 2 is a schematic of the signals, and Figure 5 shows this for a particular maneuver. Since we are interested in the aerodynamic model, and not the transfer function for the actuator or dynamics of the mechanical system, we consider the angle of attack as measured by the potentiometer as the model input.

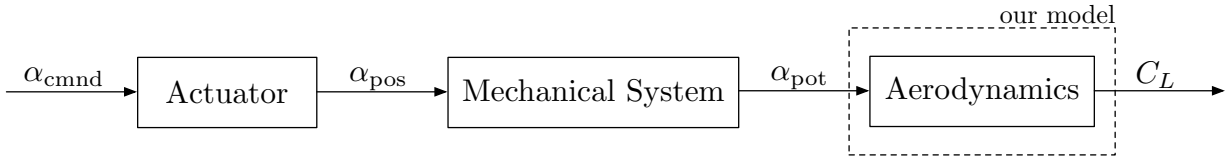

Figure 2. Schematic of wind tunnel experiment.

B. Modeling Procedure

It has been shown previously that a model of the form in Eq. 3 is effective in capturing the unsteady aerodynamic response across the full range of relative frequencies.[6,7]

$$\frac{d}{dt}\begin{bmatrix}\mathbf{x}\\ \alpha\\ \dot{\alpha}\end{bmatrix} = \begin{bmatrix}A_r & 0 & 0\\ 0 & 0 & 1\\ 0 & 0 & 0\end{bmatrix}\begin{bmatrix}\mathbf{x}\\ \alpha\\ \dot{\alpha}\end{bmatrix} + \begin{bmatrix}B_r\\ 0\\ 1\end{bmatrix}\ddot{\alpha}$$
$$C_L = \begin{bmatrix}C_r & C_{L_\alpha} & C_{L_{\dot{\alpha}}}\end{bmatrix}\begin{bmatrix}\mathbf{x}\\ \alpha\\ \dot{\alpha}\end{bmatrix} + C_{L_{\ddot{\alpha}}}\ddot{\alpha} \tag{3}$$

Here, $C_{L_\alpha}, C_{L_{\dot{\alpha}}}, C_{L_{\ddot{\alpha}}}$ are the stability derivatives and A_r, B_r, C_r is a reduced order model for the additional *fast dynamics*, obtained using the eigensystem realization algorithm. At high frequencies there are large

added-mass forces proportional to $\ddot{\alpha}$, so the input to the system must be $\ddot{\alpha}$ for the linear system in Eq. 3 to be proper in a control theory sense.

Previously, this model was constructed starting from the aerodynamic step response, or indicial response (IR), and was therefore viewed as a reduced order model of the linear indicial response model. However, the indicial response is an impulse in $\dot{\alpha}$ (step in α). To use the eigensystem realization algorithm to identify fast dynamics of the form in Eq. (3) requires an impulse in $\ddot{\alpha}$, less the contribution of the stability derivatives. It is ideal if we are able to identify this model using realistic input/output data from a simulation or an experiment instead of an idealized step response.

Now, instead of starting from the indicial response, we use the Observer/Kalman filter identification (OKID) method to identify the Markov parameters, or impulse response parameters for an impulse in $\ddot{\alpha}$. A generic set of Markov parameters for an impulse in $\ddot{\alpha}$ is shown in Figure 3. The first Markov parameter corresponds to the added-mass term $C_{L_{\ddot{\alpha}}}$ and will become the feed-through term, or D matrix, in our state-space model. Because an impulse in $\ddot{\alpha}$ is a ramp in α, we see a linear increase in H_i, and the slope is the lift slope C_{L_α} Subtracting off $C_{L_\alpha}\alpha$, the Markov parameters decay to a non-zero value corresponding to $C_{L_{\dot{\alpha}}}$, since an impulse in $\ddot{\alpha}$ is a step in $\dot{\alpha}$. Finally, after subtracting off each stability derivative, the remaining transient response is modeled using ERA.

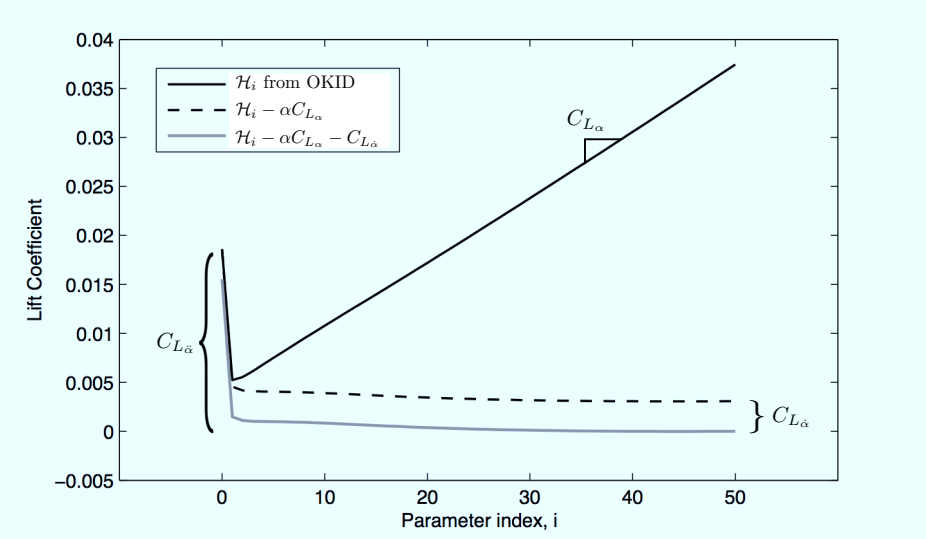

Figure 3. Markov parameters output from OKID with $(\ddot{\alpha}, C_L)$ as input/output pair (u, y).

It is important to use the form of the model in Eq 3 with $\ddot{\alpha}$ as the input to the system. If one naïvely applies the OKID/ERA method assuming the input is $\dot{\alpha}$ (so that the identified impulse response corresponds to the indicial response) then the resulting model will not respect the high-frequency added-mass. Moreover, if one considers the input of the system to be $\ddot{\alpha}$, but does not subtract off the stability derivatives from the Markov parameters, the resulting ERA system will be unstable. These issues are addressed in more detail in the literature.[7]

C. System Identification Maneuvers

The system identification (ID) maneuver for these experiments was chosen with a number of criterion in mind. Because the input to the model is $\ddot{\alpha}$, we ultimately need a maneuver with rich $\ddot{\alpha}$ content. Also, because we are identifying various stability derivatives, we need the contribution from individual changes in $\ddot{\alpha}$ to be distinguishable in the measured lift force. Finally, because the experimental measurements have noise, we require the system ID maneuver to be sufficiently aggressive so that the change in force is measureable in response to the maneuver.

The maneuver is constructed as a pseudo-random sequence of ramp-up, hold and ramp-down, hold maneuvers, related to the canonical maneuvers in Eldredge *et al.*[12,13] The equations for u and $\dot{u}$ for a single pitch-up, hold are given in Eq. (4). In this case $u = \alpha$.

$$u(t) = A\frac{G(t)}{\max G(t)}, \qquad \dot{u}(t) = A\frac{\tanh(a(t-t_1)) - \tanh(a(t-t_2))}{\max G(t)} \tag{4}$$

where

$$G(t) = \log\left[\frac{\cosh(a(t-t_1))}{\cosh(a(t-t_2))} \cdot \frac{\cosh(-at_2)}{\cosh(-at_1)}\right]. \tag{5}$$

The building block for our maneuver is shown in Figure 4.

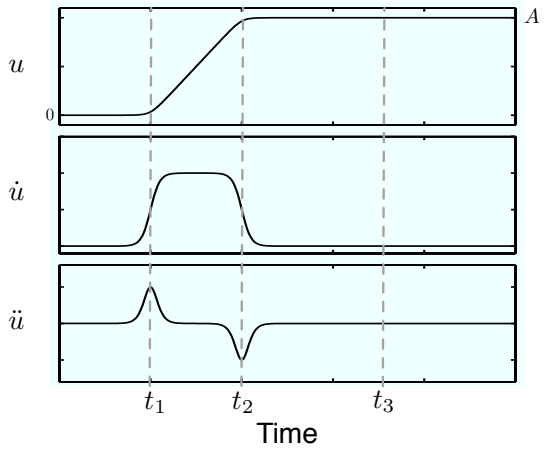

Figure 4. Pitch-up, hold maneuver.

The duration of the ramp $\tau_r = t_2 - t_1$ and hold $\tau_h = t_3 - t_2$ are bounded Gaussian white noise processes. Similarly, the step amplitude A is sampled from a normal distribution, with the constraint that the maneuver amplitude never exceeds $\pm 10°$. A maneuver of this type is attractive for a number of reasons. First, the signal $\ddot{\alpha}$ consists of pseudo-randomly spaced pulses at the beginning and end of each ramp. The result is that the large added-mass forces are similarly spaced pulses. Additionally, having a psuedo-random train of pulses in $\ddot{\alpha}$ is ideal for the OKID method. Finally, having large aggressive ramp-up and ramp-down maneuvers will result in forces large enough to measure. The command and measured angles for a particular maneuver are shown in Figure 5.

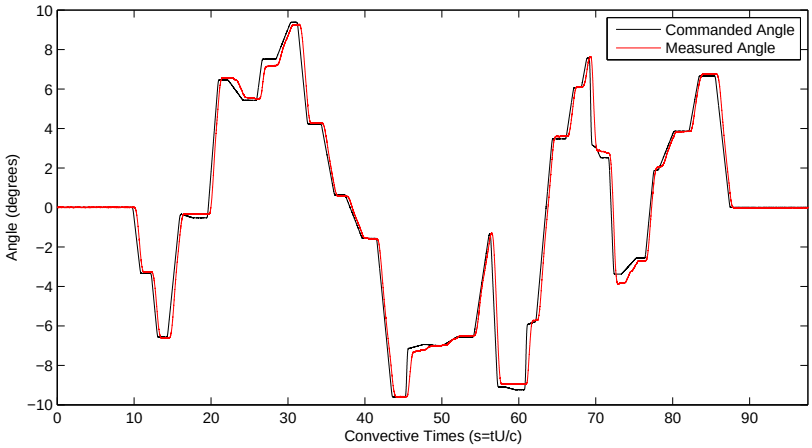

Figure 5. Example system ID maneuver; Commanded angle is $\alpha_{\mathbf{pos}}$, and measured angle is $\alpha_{\mathbf{pot}}$.

D. Phase Averaged Force Measurements

The force measurements are inherently noisy, and therefore we phase average over a number of cycles. The top of Figure 6 shows the noisy force measurements, and the bottom shows the phase averaged force.

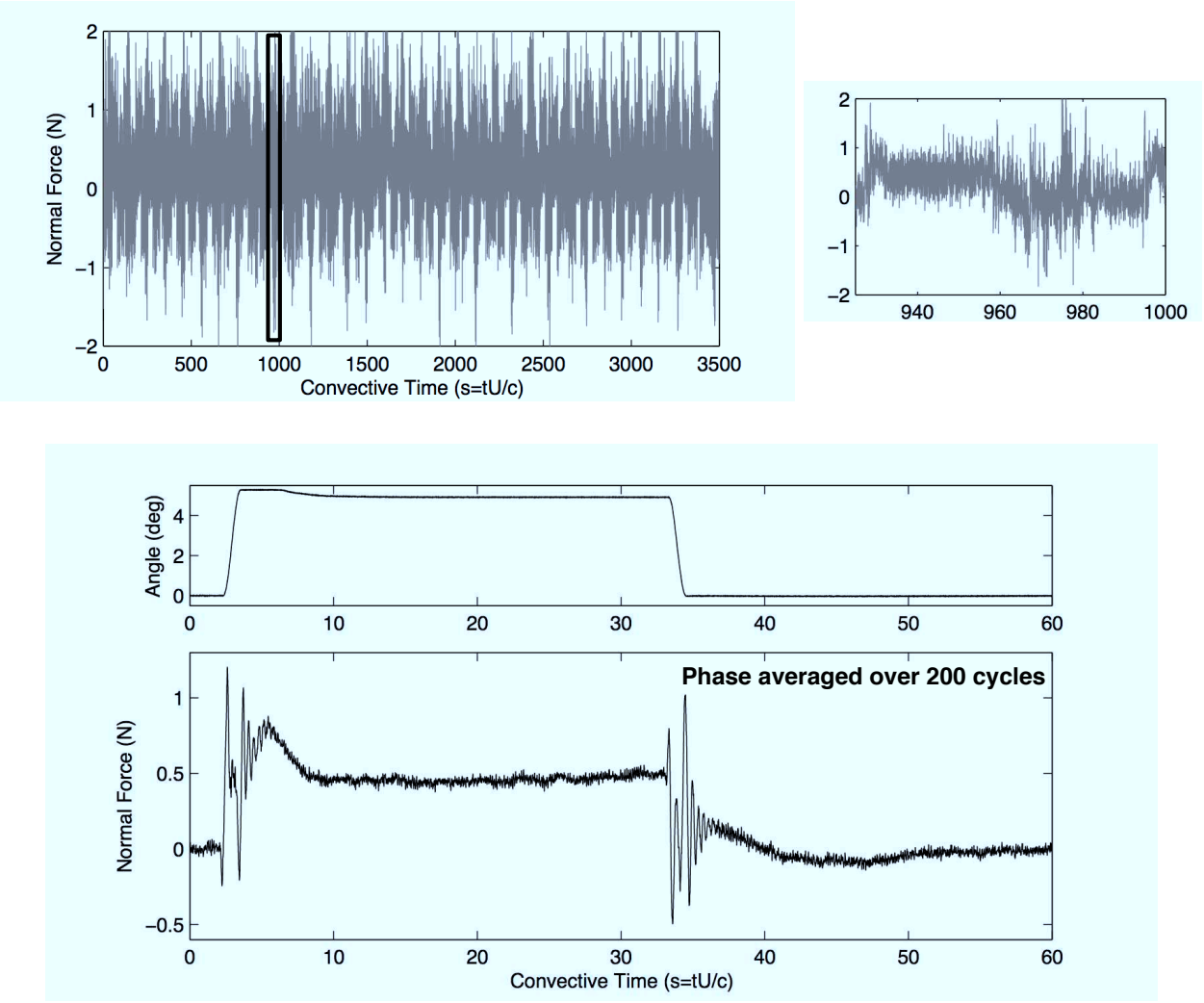

Figure 6. Phase averaged force measurement for 5 degree step-up, followed by 5 degree step-down.

Before phase averaging, we use a 6-th order Butterworth low-pass filter at 2500Hz. In addition, we coarsen the data by averaging the measurements inside each interval $[k\Delta t, (k+1)\Delta t)$, where $\Delta t = .1$ convective time unit, or .00615 seconds. Using this coarsened data as an input to the OKID method results in a discrete-time model with time-step Δt. Because the added-mass force appears as a feed-through term, it is possible to convert this to a continuous time system without loss of accuracy at high frequencies. This step is also important to ensure that the angular acceleration $\ddot{\alpha}$, as computed by finite differencing, is not too noisy.

III. Results

The following results involve constructing and analyzing reduced order models based on the system ID maneuvers discussed in Section IIC. For the case of pitching about $\alpha_0 = 0°$ and $\alpha_0 = 10°$, three pseudo-random system identification maneuvers are each used to construct a reduced order model. These models are compared in the frequency domain using Bode plots and in the time domain by how well they reproduce the force measurement from the other identification maneuvers. For every maneuver, we collect force and

position measurements for 100 identical instances of the maneuver and phase average. After phase averaging, the measured force and angle of attack measurements are discretized with $\Delta t = .1$ convective time unit, as discussed in Section IID.

A. Pitching, $\alpha_0 = 0°$

Figure 7 shows the measured angle of attack and lift coefficient for one of the pseudo-random test maneuvers, Maneuver B. The black curve is the measured force, the red curve is our reduced order model, and the green curve is Theodorsen's model. Although Theodorsen's model predicts the quasi-steady lift, it does not adequately capture the large added-mass forces.

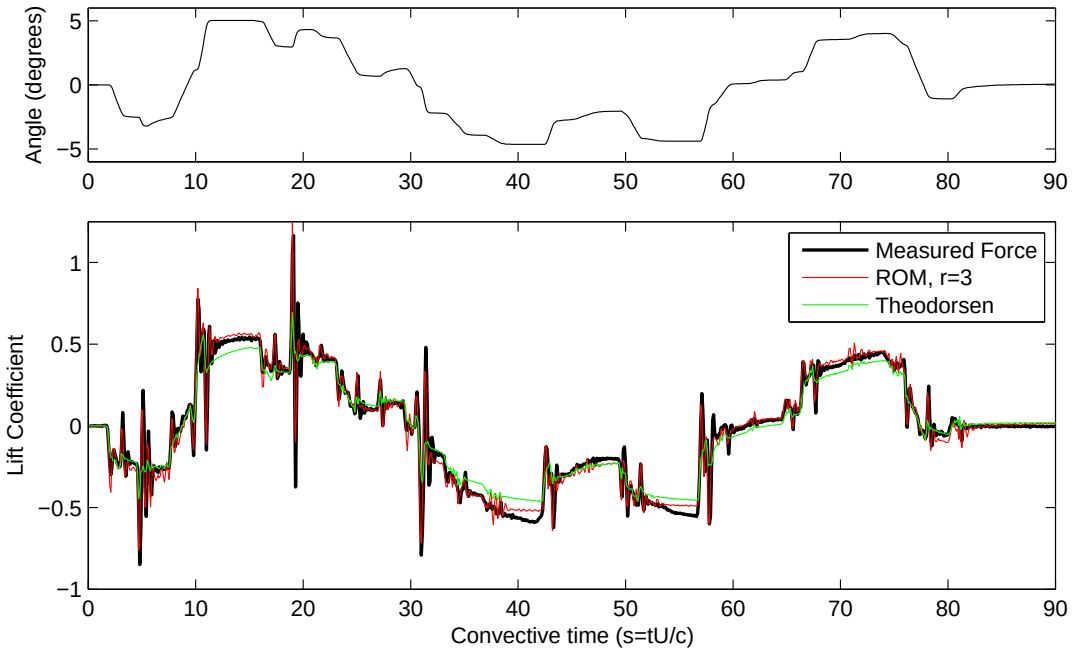

Figure 7. Measured force compared with models (bottom) for pseudo-random maneuver B centered at $\alpha_0 = 0°$ (top). A reduced order model with fast dynamics order $r = 3$ outperforms Theodorsen's model.

This procedure is repeated with similar results for three pseudo-random maneuvers, A, B, and C, which are seen in the top of Figure 8. It is possible to combine the measured response for each of the three maneuvers and obtain a model based on the concatenated signal. This model is shown in the bottom of Figure 8. Each of the maneuvers has amplitude roughly $\pm 5°$.

It is important to note that the models obtained using each system ID maneuver accurately reproduce the measured force for each of the other test maneuvers, as seen in Figure 9.

The Bode plots for each of the reduced order models based on the three system ID maneuvers, as well as the concatenated maneuver, is shown in Figure 10. All three models have similar asymptotes, corresponding to the low-frequency quasi-steady limit and high-frequency added-mass limit. In all of the models, there is a prominent resonance at around 12 rad/s $\cdot$ c/U. In dimensional units, this corresponds to around 30Hz. It is believed that this resonant peak is the result of dynamics in the mechanical system and is not aerodynamic in nature. Some ringing can be seen in Figure 6 after the fast step-up and step-down maneuver.

Finally, the Markov parameters identified using the OKID method are shown in Figure 11. In contrast to Figure 3, we notice that the added-mass forces due to $C_{L_{\ddot{\alpha}}}$ are not all lumped into the first Markov parameter, but are rather spread out over the first few parameters in an added-mass "bump". This is responsible for the "bump" in phase in the Bode plot around 5rad/s c/U. The correct modeling of this bump requires the addition of fast dynamics, since it is not entirely governed by the $C_{L_{\ddot{\alpha}}}$ term as is the case in theory and DNS. Additionally, we see some ringing in the Markov parameters.

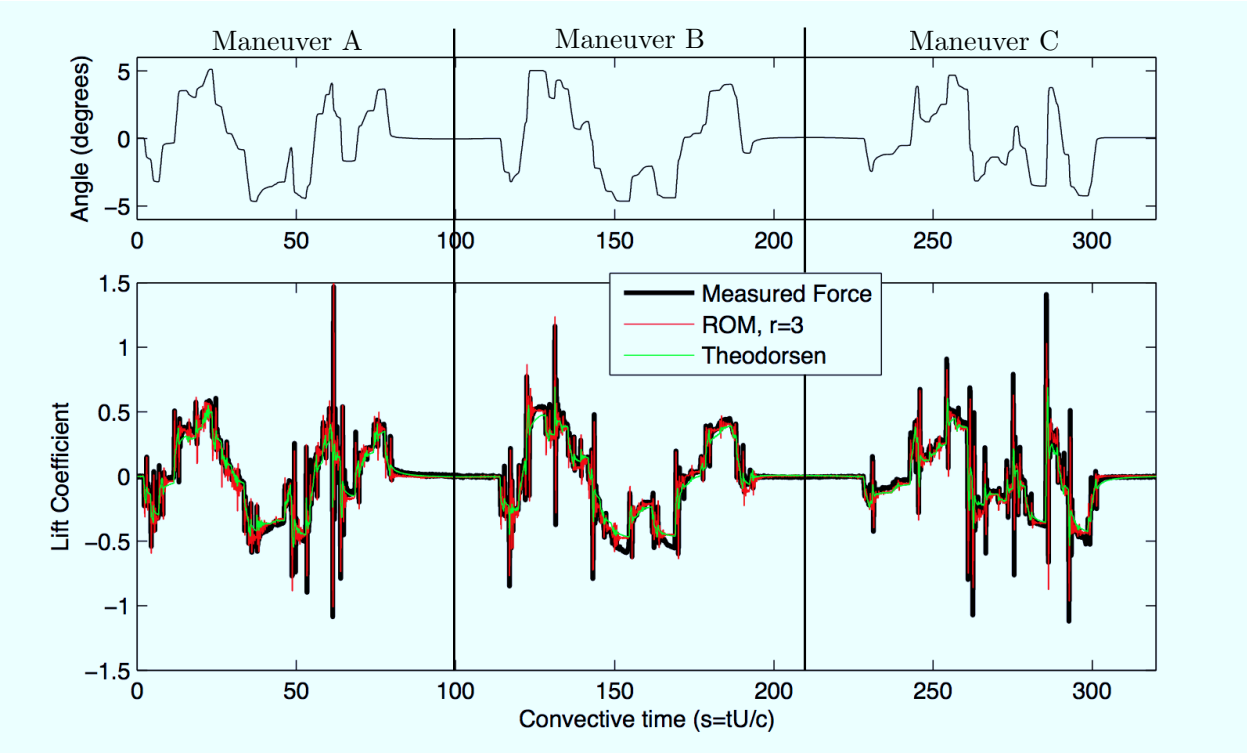

Figure 8. Response to combining all three system ID maneuvers at $\alpha_0 = 0°$. Reduced order model with fast dynamics of order $r = 3$ outperforms Theodorsen's model.

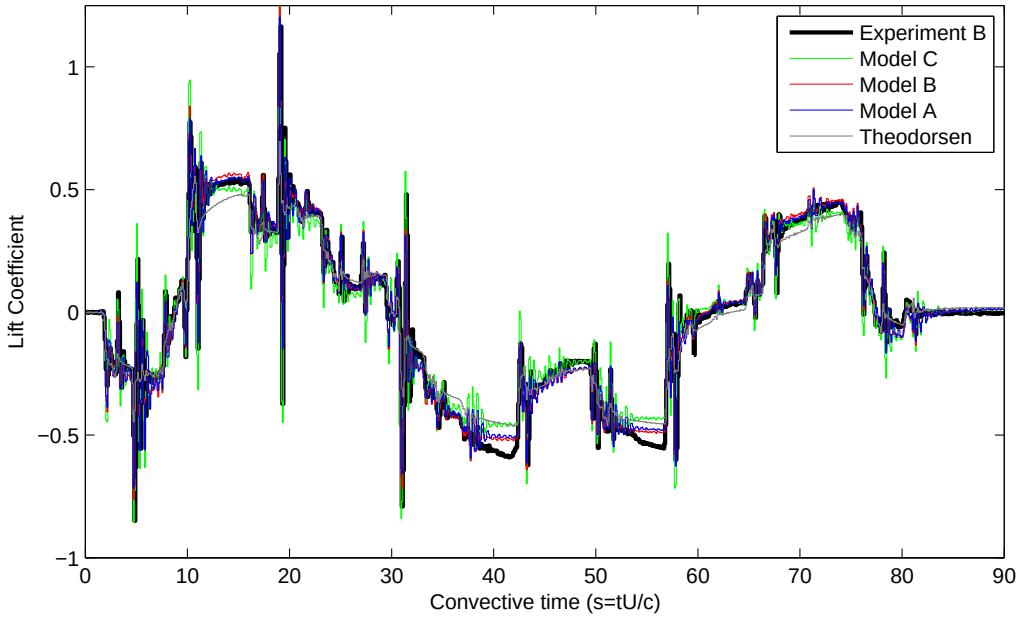

Figure 9. Performance of each reduced order model obtained on separate system ID maneuvers, applied to maneuver B.

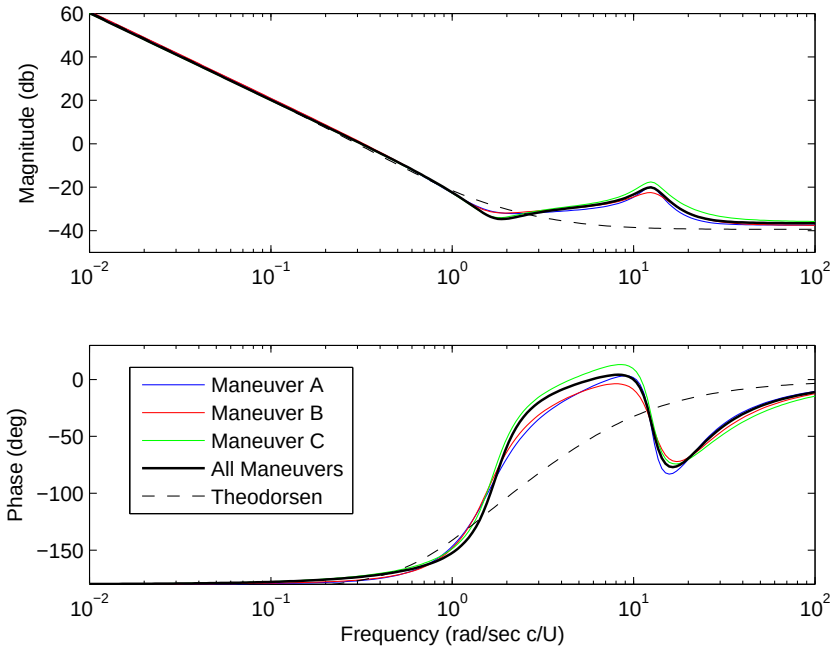

Figure 10. Bode plots for the reduced order models obtained using each of the three system ID maneuvers, and concatenated maneuver at base angle of attack $\alpha_0 = 0°$.

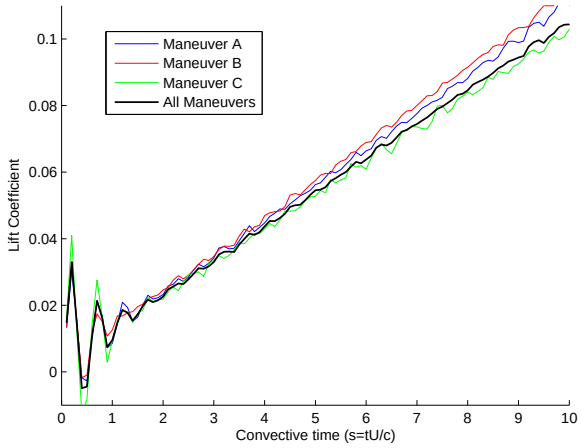

Figure 11. Markov parameters identified using OKID, for system ID maneuvers based around $\alpha_0 = 0°$.

B. Pitching, $\alpha_0 = 10°$

Here, we repeat the system identification maneuvers at a new base angle of $\alpha_0 = 10°$. In these experiments, the magnitude of the amplitude is $\pm 10°$, which is twice as large as in the previous section. Because the 2π lift slope predicted by Theodorsen is not exact for this airfoil and Reynolds number, we subtract off the steady-state error between Theodorsen's predicted lift at $10°$ and the measured lift at $10°$.

Figure 12 shows the measured response for maneuver B, along with the model prediction. The agreement of the model in Eq. (3) is not as close as in the $\alpha_0 = 0°$ case, which is most likely due to nonlinear flow effects that are not modeled. However, the model significantly outperforms Theodorsen's model.

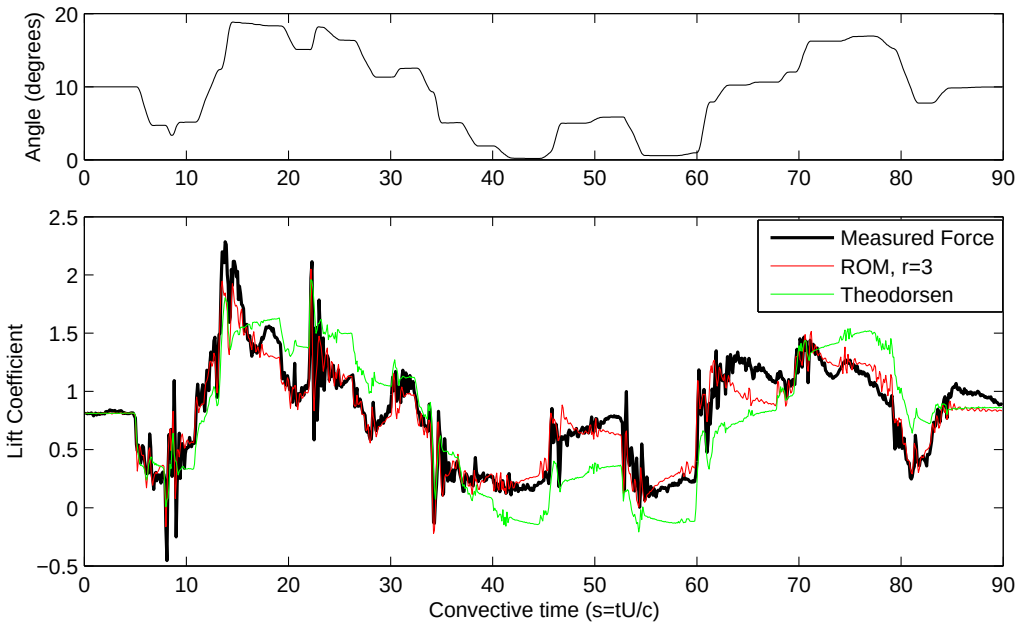

Figure 12. Measured force compared with models (bottom) for pseudo-random maneuver B centered at $\alpha_0 = 10^\circ$ (top). A reduced order model with fast dynamics order $r = 3$ outperforms Theodorsen's model.

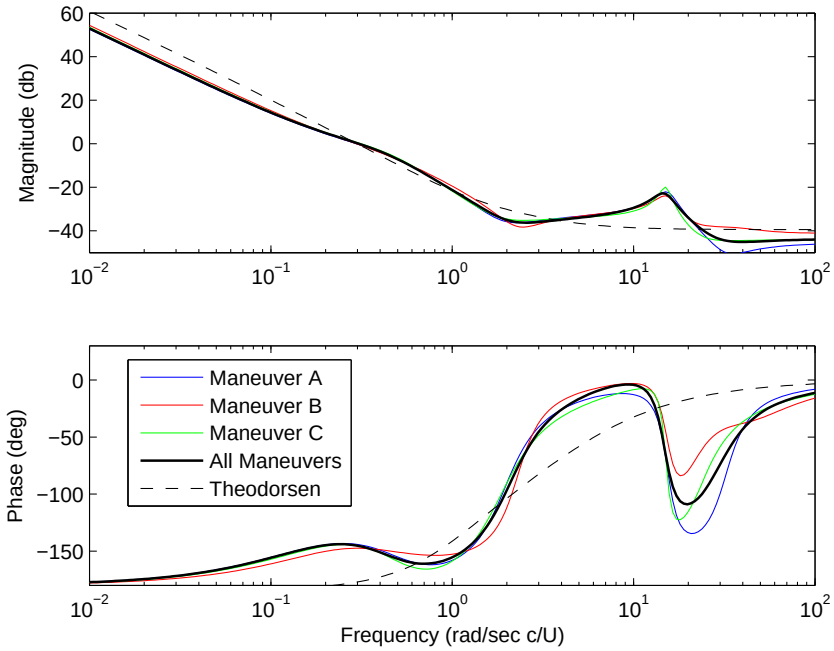

Figure 13. Bode plots for the reduced order models obtained using each of the three system ID maneuvers, and concatenated maneuver at base angle of attack $\alpha_0 = 10^\circ$.

The Theodorsen model has relatively poor quasi-steady agreement, which is due to the fact that the lift slope decreases significantly for larger angles of attack. This is seen in the decreased slope in the Markov

parameters in Figure 14 as well as in the low frequency asymptote in the Bode plot in Figure 13. Again, we see a prominent resonant peak at around 30Hz.

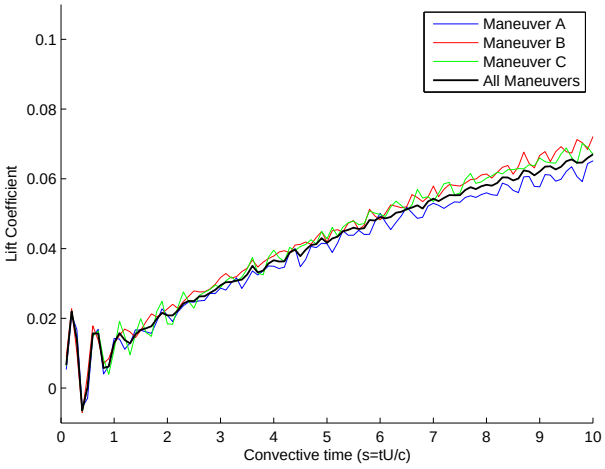

Figure 14. Markov parameters identified using OKID for maneuvers based around $\alpha_0 = 10°$.

C. Comparison of Model at $\alpha_0 = 0$ and $\alpha_0 = 10$

Figure 15 shows the Bode plots for the models linearized at $\alpha_0 = 0°$ and $\alpha_0 = 10°$. We notice that the model takes longer to reach steady state at the larger angle of attack, as illustrated by the convergence of low frequency asymptotes at lower frequencies. This effect has been seen when comparing similar models obtained in simulations at Reynolds number 100.

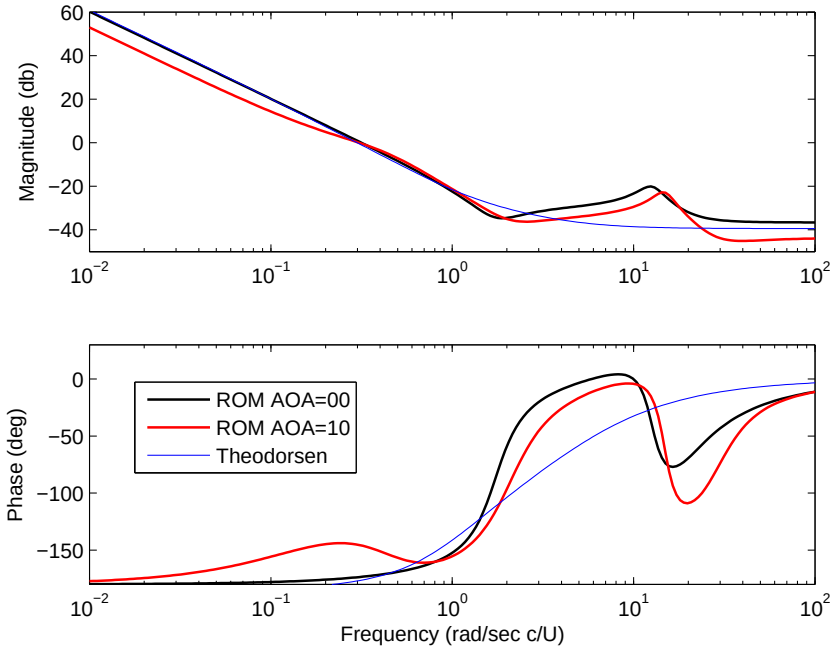

Figure 15. Markov parameters identified using OKID.

D. Model for Plunging

Figure 16 shows the model obtained for the case of pure plunge. The system ID maneuver is essentially the same as in the pitching case, except both servo tube controllers are sent the same signal. Figure 17 shows the frequency response for the pure plunge model. Again, there is a resonance at around 30Hz.

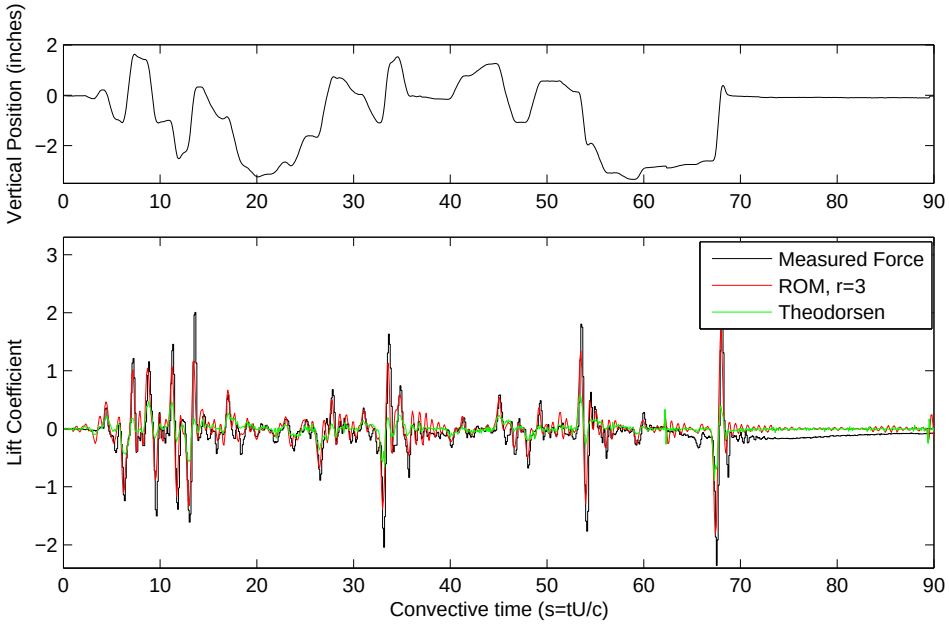

Figure 16. Measured force and model prediction for plunge maneuver using reduced order model with fast dynamics of order $r = 3$.

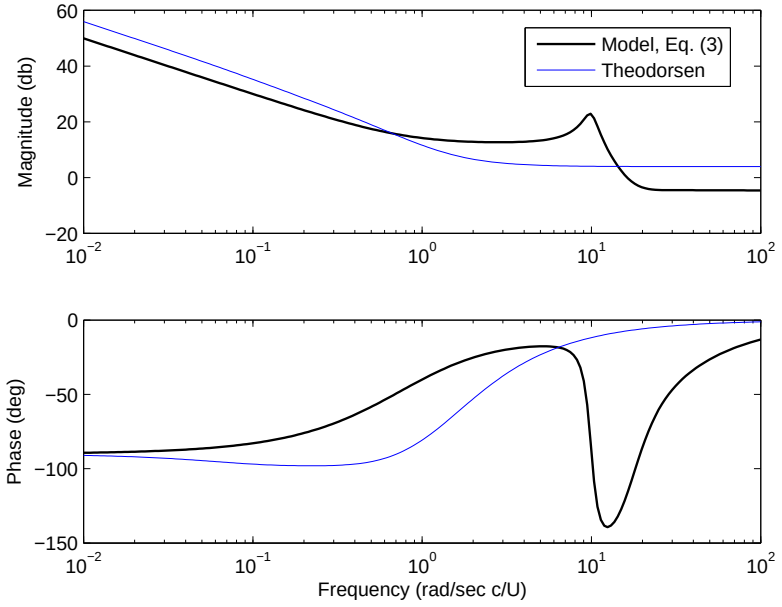

Figure 17. Bode plot of reduced order model, Eq. (3), and Theodorsen's model for plunge.

IV. Conclusions

We have demonstrated an accurate and efficient modeling procedure for developing unsteady aerodynamic models from wind tunnel measurements. To this end, we have developed a family of aggressive system identification maneuvers that excited unsteady aerodynamic responses across a range of relevant frequencies.

In the case of pitching about zero angle of attack, $\alpha_0 = 0°$, our reduced order model agrees well with the measured response. In fact, the models obtained with three different maneuvers are very similar, and are able to reconstruct the lift coefficient for each of the other maneuvers. Theodorsen's model agrees well with the quasi-steady forces, but does not capture the high frequency forces as accurately as the identified model.

The results for pitching about a non-zero angle of attack, $\alpha_0 = 10°$, are similar. However, at this angle of attack the flow is separated, and the agreement between our linear model and the measurements is not as close, presumably due to nonlinear flow effects that are not modeled. In addition, the lift slope decreases for larger angle of attack; this effect is well captured by our linear model, but is not taken into consideration in Theodorsen's model, resulting in poor quasi-steady agreement.

When comparing the models obtained at $\alpha_0 = 0°$ and $\alpha_0 = 10°$, we observe that the model takes longer to equilibrate to steady state at larger angle of attack. This can be seen by noting that the low-frequency asymptote converges for lower frequencies in the Bode plot. This effect has been seen when comparing models obtained via simulations at Reynolds number 100, and indicates a complex conjugate pair of eigenvalues approaching the imaginary axis towards a Hopf bifurcation, and subsequent coherent vortex shedding. The agreement at this larger Reynolds number suggests that the flow is still dominated by large coherent structures.

Finally, we note that in all of the models there is a significant "bump" in magnitude and phase followed by a resonant peak at around 12 (rad/sec c/U), or roughly 30Hz. It is believed that this is due to oscillations in the servo tube controllers as well as mechanical ringing in the system. It is interesting that the low order model captures these additional effects, and this is an indication that these methods may be applied more generally to aeroelastic modeling problems.

V. Acknowledgements

This work was supported by the FAA Joint University Program for Air Transportation. We also thank Vien Quatch for constructing the NACA 0006 model and Seth Buntain for help with acquiring wind tunnel data.

References

[1]Birch, J. and Dickinson, M., "Spanwise flow and the attachment of the leading-edge vortex on insect wings." *Nature*, Vol. 412, 2001, pp. 729–733.

[2]Videler, J., Samhuis, E., and Povel, G., "Leading-edge vortex lifts swifts." *Science*, Vol. 306, 2004, pp. 1960–1962.

[3]Wagner, H., "Über die Entstehung des dynamischen Auftriebes von Tragflügeln," *Zeitschrift für Angewandte Mathematic und Mechanik*, Vol. 5, No. 1, 35 1925, pp. 17.

[4]Theodorsen, T., "General theory of aerodynamic instability and the mechanism of flutter," Tech. Rep. 496, NACA, 1935.

[5]Brunton, S. L. and Rowley, C. W., "Low-dimensional state-space representations for classical unsteady aerodynamic models," *49th AIAA Aerospace Sciences Meeting and Exhibit*, 2011.

[6]Brunton, S. L. and Rowley, C. W., "Reduced-order model for unsteady aerodynamic forces based on the indicial response," submitted to *AIAA Journal*, 2011.

[7]Brunton, S. L. and Rowley, C. W., "Linear models for unsteady aerodynamics at high angle of attack," submitted to *AIAA Journal*, 2011.

[8]Juang, J. and Pappa, R., "An eigensystem realization algorithm for modal parameter identification and model reduction," *Journal of Guidance, Control and Dynamics*, Vol. 8, No. 5, 1985, pp. 620–627.

[9]Ma, Z., Ahuja, S., and Rowley, C., "Reduced order models for control of fluids using the Eigensystem Realization Algorithm," *Theoretical and Computational Fluid Dynamics*, Vol. 25, 2009, pp. 233–247.

[10]Jer-Nan Juang, Minh Phan, L. G. H. and Longman, R. W., "Identification of Observer/Kalman Filter Markov Parameters: Theory and Experiments," Technical Memorandum 104069, NASA, 1991.

[11]Juang, J.-N., *Applied System Identification*, Prentice Hall PTR, 1994.

[12]Eldredge, J. D., Wang, C., and OL, M. V., "A computational study of a canonical pitch-up, pitch-down wing maneuver," *39th AIAA Fluid Dynamics Conference*, June 2009.

[13]OL, M. V., Altman, A., Eldredge, J. D., Garmann, D. J., and Lian, Y., "Résumé of the AIAA FDTC Low Reynolds Number Discussion Group's Canaonical Cases," AIAA Paper 2010-1085, 2010.